# Heat transfer enhancement in laminar flow by a protrusion in a rectangular channel

**Author:**
Alshroof, Osama; Reizes, John; Timchenko, Victoria; Leonardi, Eddie

**Publication details:**
International Symposium on Advances in Computational Heat Transfer

**Event details:**
International Symposium on Advances in Computational Heat Transfer
Morocco

**Publication Date:**
2008

**DOI:**
https://doi.org/10.26190/unsworks/389

Proceedings of CHT-08
ICHMT International Symposium on Advances in Computational Heat Transfer

May 11-16, 2008, Marrakech, Morocco

CHT-08-404

# HEAT TRANSFER ENHANCEMENT IN LAMINAR FLOW BY A PROTRUSION IN A RECTANGULAR CHANNEL

O. Alshroof*, J. Reizes, V. Timchenko and E. Leonardi
School of Mechanical and Manufacturing Engineering
The University of New South Wales
Sydney, NSW 2052, Australia
*Corresponding Author. Fax: +61 2 9663 1222 Email: o.alshroof@unswalumni.com

**ABSTRACT** A numerical investigation has been performed to determine the effect on heat transfer in the laminar regime of introducing a single protrusion in a rectangular channel. The geometry consists of a three dimensional channel 10 *mm* high, 40 *mm* wide and 290 *mm* long in which a spherical protrusion was placed 90 *mm* from the inlet on the centreline of one of the wide sides. The print diameter of the obstacle was equal to the height of the channel and it protruded 2.2 *mm* above the surfaces. In order to properly take into account developing flow, a 30 *mm* region was introduced upstream of the inlet. Adiabatic wall with zero shear stress boundary conditions were used on all four walls of this region and uniform velocity and temperature distributions were assumed at the inlet of the calculation region. The two wide plates of the channel and the protrusion were set to 45ºC and the other two sides adiabatic. The fluid was assumed to be silicon oil with an inlet velocity of 1 $ms^{-1}$ at a temperature of 20ºC, yielding a Reynolds number of 1600 based on the hydraulic diameter of the channel. A commercial code, ANSYS-CFX11.0 was used for all simulations. The resultant very complex flow and thermal fields in the channel are discussed in detail. The presence of the protrusion results in an enhancement in the total heat transfer rate of 7% above that of a channel lined with flat plates only. This is a worthwhile increase since it is brought about by a pressure increase of only 1%.

## NOMENCLATURE

| | |
|---|---|
| $D$ | print diameter of the protrusion |
| $h$ | height of the protrusion |
| $H$ | height of the channel |
| $Re_D$ | Reynolds number = $D\ U_\infty / \nu$ |
| $Re_h$ | $Re_h = h\ U_\infty / \nu$ |
| $Re_H$ | $Re_H = U_\infty H/\nu$ |
| $Re_x$ | $\mathrm{Re}_x = U_\infty x / \nu$ |
| $U_\infty$ | free stream velocity upstream of the channel |
| $u$ | velocity in the direction parallel to channel walls |
| $v$ | velocity in the direction perpendicular to the bottom wall |
| $w$ | transverse velocity |
| $0$ | origin of coordinate system |

| | |
|---|---|
| $x$ | coordinate in the direction parallel to channel walls |
| $y$ | coordinate in the direction perpendicular to the bottom wall. |
| $z$ | coordinate in the direction perpendicular to the side wall. |

## INTRODUCTION

The performance of many devices, from air conditioning plants through power stations to computers is dependent on the effectiveness of heat transfer. It follows that there have been many attempts at enhancing heat transfer from a given area whilst minimizing undesirable concomitant changes of other aspects of performance, particularly the pressure drop. One apparent method of heat transfer enhancement is to introduce dimpled and/or protruded surfaces. Numerical and experimental studies of heat transfer from the dimpled and/or protruded surfaces have mostly concentrated on analysing the flow structure and enhancement of heat transfer in turbulent flows, for example Belen'kiy *et al* [1991], Ekkad *et al* [2003], Mahmood *et al* [2001, 2003], and Terekhov *et al* [1997]. The literature on laminar flows over such structures is much more limited.

Laminar flow structures over a single spherical dimple on a flat plate with a rounded edge were studied numerically by Isaev *et al* [1997, 2001] in the dimple Reynolds number, $Re_D$, range $100< Re_D <2500$, in which $Re_D = U_\infty D/\nu$, where, $D$ is the dimple imprint diameter, $U_\infty$ is the velocity outside the boundary layer and $\nu$ is the kinematic viscosity. Unfortunately, there is no mention of either the position of the dimple along the plate or, what is equivalent, the Reynolds number based on the distance from the leading edge, $x$, viz, $Re_x = U_\infty x/\nu$. Instead, Isaev *et al* used the thickness of velocity boundary layer equal to the dimple depth, $h$, and the Polhausen velocity distribution as the boundary condition at the inlet of their calculation domain, which was located $5D$ upstream of the dimple centre. This approach reduces the region over which numerical calculations needed to be performed. They emphasised that at low $Re_D$, $Re_D$ ~100, the motion of fluid is directeds from the centre of the dimple to its periphery and remained essentially two-dimensional. As the dimple Reynolds number is increased, separation of the flow becomes three-dimensional and jet-like vortical flows form. The fluid from the periphery now moves to the central axial plane of the dimple and is ejected in the general direction of flow in an area adjacent to it. Although there are descriptions and a discussion of the flow fields, only a few quantitative values are actually presented, consisting of the maximum absolute cross-flow velocity component parallel to the plate at $Re_D$ 100 and 2500.

Alshroof *et al* [2007] studied the same problem as Isaev *et al* [1997, 2001]. In order to obtain reliable results, Alshroof *et al* [2007] showed that a much more thorough approach is necessary in terms of mesh refinement and boundary conditions, than that used by Isaev *et al* [1997, 2001]. As a consequence, Alshroof *et al* [2007] found that in the range of $700\leq Re_D\leq 3000$ the total heat transfer from the surface with a single dimple is reduced below its values on a smooth flat surface. This contrasts sharply with the claim by Isaev and his co-workers that heat transfer is increased in the same Reynolds number range by the presence of a dimple. Interestingly, despite the reduction in the overall heat transfer rate found by Alshroof *et al* [2007], because there is a reduction in the shear stress over the dimple, the thermal performance factor, defined as the ratio of the fractional increase in the heat transfer rate to the fractional increase in the average sheer stress, is marginally increased by a maximum of approximately 4%.

Khalatov *et al* [2004], studied experimentally and numerically the flow structures and heat transfer within, and downstream of single spherical and cylindrical dimples. In particular, they investigated a shallow dimple with depth to imprint diameter ratio, $h/D$, equal to 0.1, in laminar and turbulent flows in the range $3{,}000< Re_D< 23{,}600$. In the laminar regime they found that, the ratio between the

heat transfer coefficients on the plate with the dimple decreased immediately downstream of the dimple. From 0.5*D* to 2.38*D* downstream of the dimple, the ratio increased to a maximum, then reduced so that at around 5-6*D* downstream the effect of the dimple was no longer discernable. This is in general agreement with the results obtained by Alshroof *et al* [2007], but it is not clear whether Khalatov *et al* [2004] found that at the lower Reynolds numbers there is also a reduction in the overall heat transfer.

The problem of the dimple and protrusion heat transfer enhancement is changed by the introduction of boundaries, such as may be found in heat exchangers. Ligrani *et al* [2001] experimentally studied the flow structures and local Nusselt number development in a rectangular channel with dimples on one wall and protrusions on the opposite wall. The dimples and protrusions were placed on the wide walls of the channel. Four relative offset positions were studied between dimples in one surface and protrusions on the other. The ratio of channel height to dimple and protrusion print diameter was 0.5, with a dimple and protrusion depth to print diameter of 0.22, and the channel Reynolds number, $Re_H = U_\infty H/v$, in the range $380<Re_H<30{,}000$, in which $H$ is the channel height. In each case, the presence of protrusions had a significant impact on flow structure and heat transfer. They claimed that six vortex pairs were present downstream of each dimple protrusion combination, and a large proportion of flow was forced into dimple cavities, resulting in significant mixing even at low Reynolds numbers. This led to a considerable augmentation of local heat transfer over the dimpled surface. Unfortunately, the pressure drop was increased by a factor between 2 and 2.7 of that which pertained when a flat surface was used opposite the dimpled wall. This result might have been expected since there appears to be no heat transfer through the protrusion which, whist acting to enhance the heat transfer in the dimples also are significant obstructions to the flow without themselves taking part in the heat transfer process. Therefore it appears to be an unfair judgment as to the morrit of the effects of protrusions.

Similarly, Leontiev *et al* [2006] studied the flow and heat transfer in channels with spherical dimples and proposed 'models' of flow separation in the laminar regime which were functions of the dimple parameters and $Re_h$, the Reynolds number based on the dimple depth. As $Re_h$ is increased, the flow appears to separate with the formation of the symmetric vortices about the central axial plane of the dimple. Further increasing $Re_h$ led to an increase in the length of the recirculation zone. Toroid-like vortexes were observed experimentally for the deep dimples in shallow channels.

Mahmood *et al* [2001] extended the work of Ligrani *et al* [2001] by investigating three configurations of dimple-protrusion in a channel in which dimples were located at one surface and flat, misaligned or aligned protrusions on the opposite surface. The channel aspect ratio was equal to 16, the channel height to dimple print diameter was 0.5, and dimple depth to dimple print diameter was 0.2 where the dimple diameter was 5.08 *cm*. The same values where used for protrusions. The Reynolds number based on channel height was in the range from $5\text{x}10^3$ to $3.5\text{x}10^4$. The authors indicated a reduction in average heat transfer enhancement with increasing Reynolds numbers when protrusions were placed on the opposite wall, whilst in the case of the smooth opposite surface a change in average heat transfer was less dependent on Reynolds number. The increase of the thermal performance parameter by replacing the flat surface with protruded one, varied from 1.45 to 1.55 depending on the value of Reynolds number.

Wang *et al* [2003] studied laminar flow in a 1*D* high, 1.62*D* wide and 8*D* long channel with a dimple placed in the centre of the bottom surface. A parabolic velocity profile was imposed at the inlet boundary condition, with an outflow boundary condition at the outlet, in the span-wise direction periodic boundary condition was employed. Two parametric ratios of dimple depth to its print diameter were investigated, viz, 0.1 and 0.2, in which it was placed at the middle of the computational domain. They investigated the effect of Reynolds number, based on the maximum

velocity and channel height on the flow separation in and around the dimple. No separation below Re=100 “based on maximum velocity” was observed. The flow separates at Re>100 and the separation region grows as the Reynolds number increases. These results qualitatively match the results of many researchers including those of Isaev *et al* [1997, 2001]. In this geometry the bounding walls are so close to the dimple that the results of Wang *et al* [2003] would not appear to have general applicability.

A situation which appears to be of more general interest was investigated by Hwang *et al* [2007] who experimentally studied the heat transfer and pressure drop in a rectangular channel with various combinations of dimpled, protruded and dimpled-protruded on the opposite wide walls of the conduit. The channel Reynolds number based on the hydraulic diameter was, in each case, fixed at $10^4$. Similarly to the results obtained by Alshroof *et al* [2007], Mahmood *et al* [2001] and Ligrani *et al.*[2001], a high heat transfer region was observed on the back surface of the dimple whereas, because of the separation, the remainder of the dimple surface had a low heat transfer flux. For the protruded surface, horseshoe vortices were generated thereby enhancing heat transfer on the front surface of the protrusion. On the other hand, a low heat transfer region existed on the back surface of the protrusion due to the wake downstream of the obstacle. The highest heat transfer flux occurred on the protruded surface, but, as may have been expected, this was also the area of maximum sheer stress. As a consequence, the dimpled surface had the highest performance factor whose value was approximately 1.4, whereas it was 1.15 for the combined dimple-protruded surface and merely 1.05 for the protruded surface only.

Despite all the above work, there is contradictory data which is based on differently defined Reynolds numbers, so that it is clear that the information is insufficient for determining whether dimpled or protruded surfaces enhance heat transfer in heat exchangers, particularly in small channels in which the flow is likely to be laminar. There is only a small increase, in fact, possibly a decrease in the heat transfer rate when dimples are used in an attempt to enhance heat transfer in laminar flows consequently, protrusion appear to show more promise, despite a likely increase in pressure drop. A numerical study was therefore undertaken on the flow and heat transfer in the vicinity of an isolated protrusion in a rectangular channel so as to obtain adequate information for the development of heat exchangers employing protrusions to enhance heat transfer.

## DESCRIPTION OF THE PROBLEM

As shown in Figure 1, a spherical protrusion whose print and height diameter are 10 *mm* and 2.2 *mm* respectively, is located on the axial centreline of the lower surface of a rectangular channel. The centre of its print diameter is at a distance 90 *mm* from the inlet. The channel is 290 *mm* long, 40 *mm* wide and 10 *mm* high. Silicon oil with a kinematic viscosity of $1x10^{-5}$ *m^2s^-1* flows from left to right with a velocity of 1.0 $ms^{-1}$. Also shown in Figure 1 is a 30 *mm* long region in front of the inlet. This region is needed so as to avoid difficulties with boundary conditions at the inlet to the channel itself, this approach has been discussed in detail by Alshroof *et al* [2007].

## SIMULATION METHODOLOGY

**Mathematical Model** Three-dimensional computations of laminar incompressible flow were performed for the configuration shown in Figure 1. The problem was solved by obtaining the instantaneous temperature and velocity fields in the channel by using a commercial package, ANSYS CFX-11.0. The transient incompressible flow of silicon oil has been simulated by the use

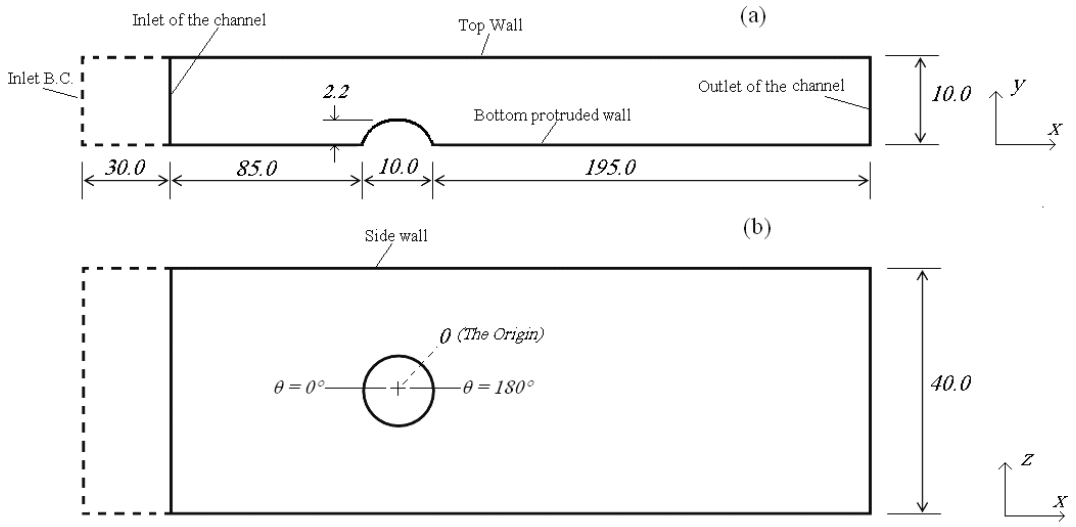


Figure 1 Schematic diagram of computational domain. (a) elevation and (b) plan views. All dimensions are in *mm.*

of the conservation equations consisting of the equation of continuity.

$$\nabla \cdot \tilde{V} = 0 \tag{1}$$

the Navier-Stokes equation,

$$\rho \frac{\partial \tilde{V}}{\partial t} + \rho \nabla \cdot (\tilde{V}\tilde{V}) = -\nabla p + \mu \nabla^2 \tilde{V} \tag{2}$$

and the energy equation,

$$\rho c_p \frac{\partial T}{\partial t} + \rho c_p \nabla \cdot (\tilde{V} T) - k \nabla^2 T = 0 \tag{3}$$

in which, $\rho$, $c_p$, $\tilde{V}$, $p$, $\mu$, $h$, $T$, $k$, and $t$ denote density, specific heat, velocity vector, gauge pressure, dynamic viscosity, absolute temperature, thermal conductivity and time respectively.

**Boundary Conditions** The sidewalls were modelled as adiabatic, whereas the top and bottom walls were set at a constant temperature of 45˚C, with the no slip wall boundary condition applied to all channel walls. A constant velocity profile at 1 *ms^-1* together with a constant temperature of 20˚C and zero average gauge pressure were imposed at the inlet to the domain, in which it was shifted 3*D* upstream of the channel entrance as is shown in Figure 1. A constant mass flow rate was set as the outlet boundary condition. Adiabatic and zero shear stress conditions were imposed on all four bounding surfaces between the inlet to the computational domain and actual channel entry. The origin of the coordinate system of the geometry is located at the centre of the protrusion print diameter on the lower channel surface and is marked as *0* in Figure 1(b).

**Details of the Grid** A combination of two types of grids have been used to discretise the equations. Firstly, an O-grid centered on the protrusion and enclosing an area 2*D* in diameter is presented in plan view in Figure 2. A very fine “body fitted” mesh was employed perpendicular to the bottom wall and protrusion surfaces. Secondly, a hexahedral grid was used in the remainder of the computational domain. As shown in Figures 3, the grid was concentrated over the protrusion and its surrounds so as to adequately resolve the complex flow structures around the protrusion. The origin of the coordinate system of the geometry is located at the centre of the protrusion print diameter on the lower channel surface and is marked as *0* in Figure 1(b). All lengths in this paper are expressed in *mm* unless otherwise indicated. When the total number of cell points was $3.18 \times 10^6$, the smallest cell size was 0.0476 x 0.0214 x 0.0492 and the maximum size was 2.6 x 0.921 x 0.478. A second order backward Euler differencing scheme was used for the transient term, and a second order

upwind differencing scheme was employed for the advection terms in the Navier-Stokes equation. If the flow about the protrusion was steady, the solution was deemed to have converged when the residuals of all equations had been reduced to $10^{-8}$. However, if the flow about the obstacle was unsteady, internal iterations were continued until the mass, momentum and energy residuals had been reduced to $10^{-6}$ at each time step. In order to determine whether the flow was steady or not, a transient calculations was performed. In a flow-time of $7 \times 10^{-5}$ *s* the solution converged to steady values on each of the meshes used. The converged solutions were then disturbed but, after going through a transient period, a steady flow was again predicted which differed by only a small fraction of a percent from the earlier results.

A grid convergence study was undertaken in order to choose an appropriate mesh size. Velocity values at the point (70, 1.5, 0) and heat flux at a point on the protrusion surface at (0, 2.2, 0) as a function of grid size are plotted in Figure 4. It is seen that, when $3.18 \times 10^{6}$ grid points were employed, the velocity and the heat flux had very nearly reached their asymptotic values, therefore, the results obtained on this mesh were deemed sufficiently accurate.

Now that the problem has been fully defined, and an appropriate mesh chosen, it is possible to discuss the results which have been obtained.

## RESULTS AND DISCUSSION

Since buoyancy effects have not been included in the calculation, the velocity distribution is independent of the temperature distribution. It follows that the temperature distribution is completely controlled by the velocity field and the thermal boundary conditions. It further follows that the flow field needs to be discussed first so as to make the thermal fields and heat flux distribution understandable.

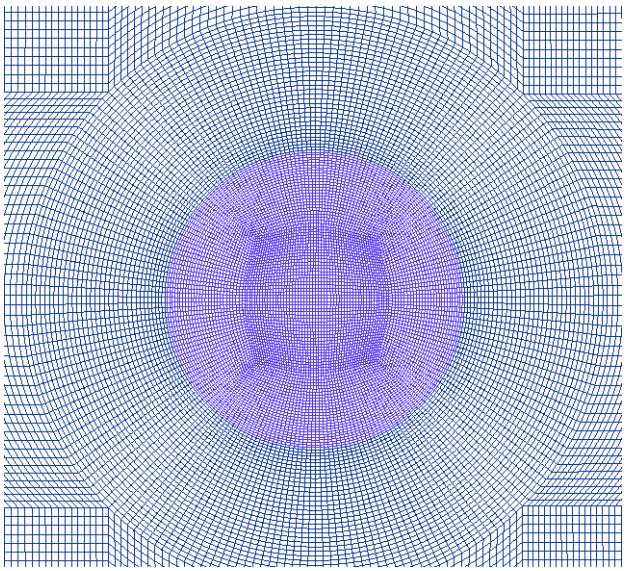

Figure 2. Plan view of the mesh on the protruded surface.

(a)

(b)

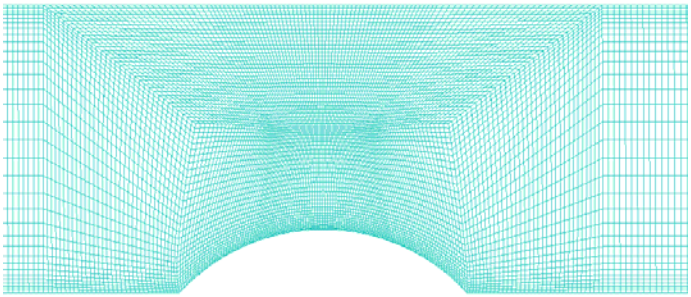

Figure 3. Elevation of the mesh at the centre longitudinal plane for (a) full channel and (b) enlarged view near protrusion.

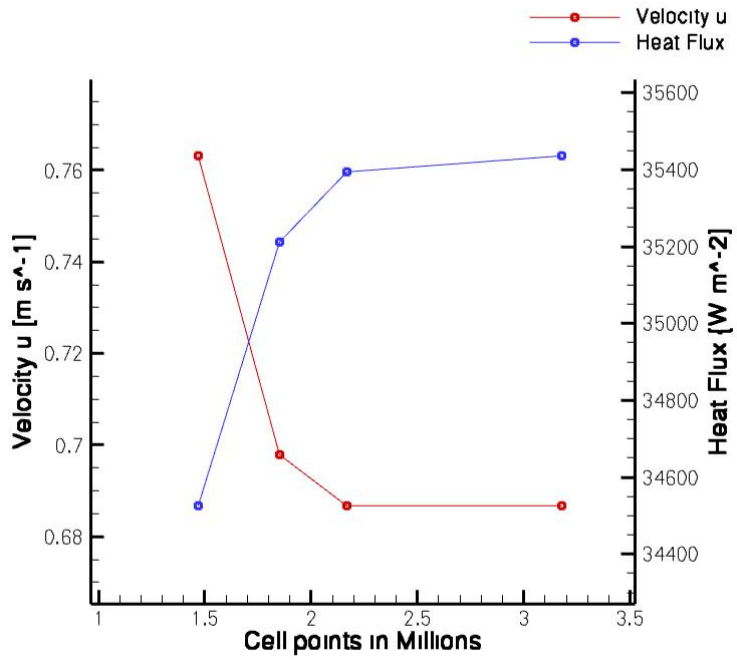


Figure 4. Grid convergence study for velocity at (70, 1.5, 0), and heat flux at (0, 2.2, 0) as a function of mesh cell points

**Flow Fields** In order to make the flow structures around the protrusion easier to describe, as may be seen in Figure 5, different parts of the flow are discussed in terms of the areas through which the fluid passes on the plane normal to the axis of the channel located 15 upstream of protrusion print centre, *0*. The non-dimensional coordinates (*z, y*) shown in Figure 5 have been normalised with the print diameter of the protrusion. The fluid passing through each of the regions is initially tracked individually and then its pattern is coupled with other streams thereby enabling the interaction between the various streams to be clearly delineated. The flow topology is then used to explain the resultant heat flux distribution in the vicinity of the obstruction.

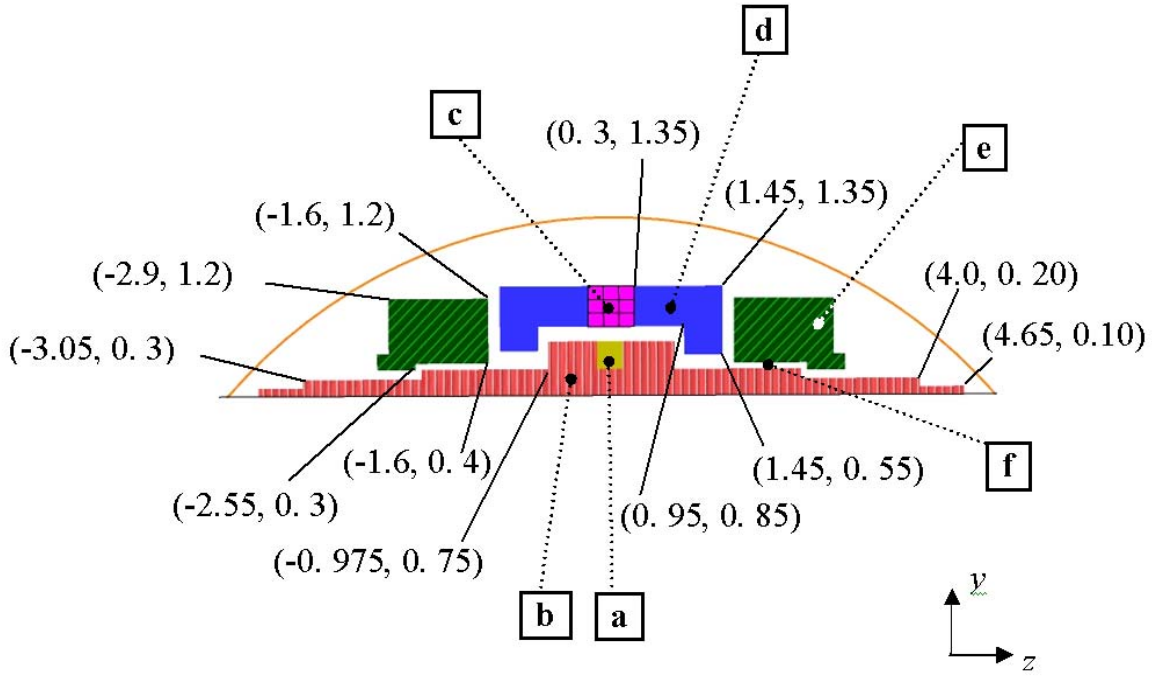


Figure 5. Diagram of locations of various streams of fluid on a plane perpendicular to the channel axis 15 upstream of the origin.

The flow passing through the nearly square region "a", defined by $0.35 \leq y \leq 0.75$ and $-0.3 \leq z \leq 0.3$ in Figure 5, is represented by the dark yellow streamlines in Figure 6. Unlike, Hwang *et al* [2007], a horseshoe vortex does not form upstream of this small obstruction. Since this flow is within the boundary layer, the highest stagnation pressure occurs further up the protrusion, in the region coloured red Figure 7, forcing the flow represented by the yellow streamlines to change direction towards the bottom surface of the channel. But this pressure difference is not large enough for a horseshoe vortex to form. This stream then splits into two symmetric flows, one on either side of the protrusion.

The fluid then follows around the protrusion, and as may be seen in Figure 6(b) it becomes an almost vertical stream. At about 120° it begins to rise and move toward the central longitudinal plane of the channel as it enters the separation region about 10 behind the protrusion. Because of the low pressure in the separation region, this fluid moves further towards the axis of the channel and as it continues to rise, its velocity reverses, as indicated by the yellow arrow in Figure 6(a), so that it now flows toward the protrusion.

The fluid continues to rise as it moves toward the obstacle from the downstream direction until it becomes affected by the fluid flowing above the separation; so that, as shown by the gray arrow in Figure 6a, the flow direction reverses for the second time and the fluid once again moves in the downstream direction at about 1.5 from the lower wall with a velocity vector more or less parallel to the side and lower walls of the channel. However, the fluid which originally passed through area "a" now flows as two ribbons, inclined at approximately 20˚ to the vertical direction, on either side of the central longitudinal plane of the channel.

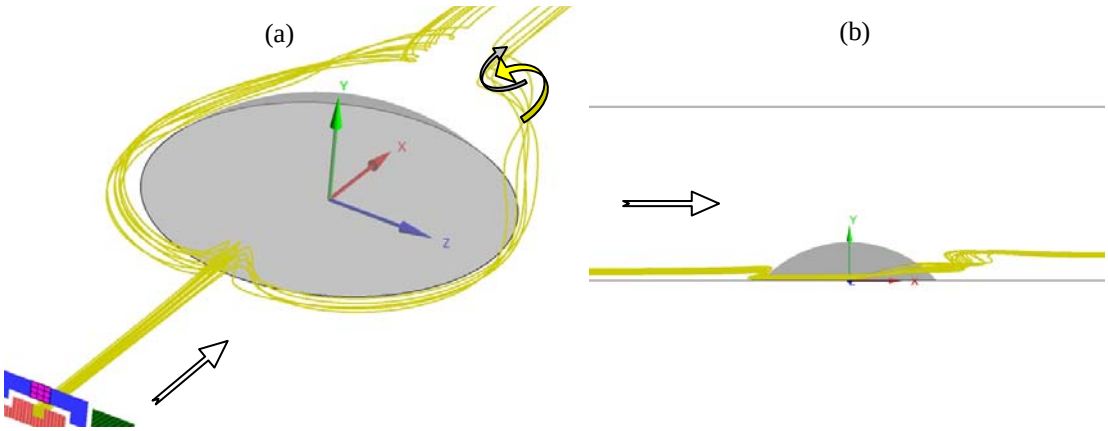


Figure 6. Streamlines of fluid passing through region “a”:
(a) 3-D view, (b) side view.

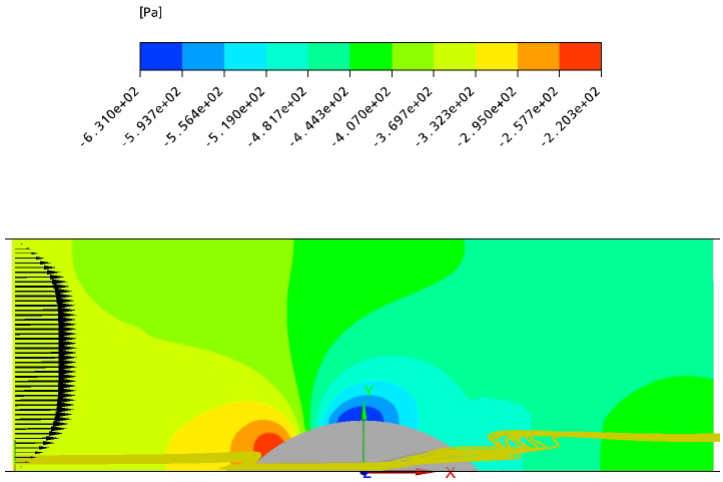


Figure 7. Pressure distribution on the central longitudinal plane of the channel, velocity distribution 15 upstream of the origin and side view of streamlines of fluid passing through region “a”.

Meanwhile, as may be seen in Figures 8, the essentially horizontal ribbon of fluid flowing through region “b” in Figure 5, which initially flowed below and beside the fluid in region “a”, continues at the same level around the protrusion. At about 130˚ around the protrusion some of the fluid, which had passed through area “b”, begins to wrap itself around the fluid which had passed through region “a”. It then follows much the same path as that taken by the region “a” fluid. The rest continues at the same level, to enter the separated region further downstream, after which, it changes its direction and lifts from the bottom surface, as may be seen in Figure 8(a). The fluid from region “a” is located near the main cross-stream vortex in the separation, whereas the fluid from region “b” moves within and around that vortex. Therefore the fluid coming from region “a” is surrounded by the fluid crossing region “b” within and downstream of the separated region, so that it fills the space between the two ribbons from region “a” downstream of that region.

On the other hand, as shown in Figures 9 (a) and (b), the fluid which crosses region “c” (Figure 5), located above region “a”, flows over the front and top of the protrusion but, as expected, separates and continues to move, as shown in Figure 9 (b), more or less horizontally downstream of the protrusion over the fluid which had originally passed through region “a”. Because the flow is laminar and steady, there is no mixing between these streams all the way to the exit from the computational domain. As shown in figure 9(c), on the central longitudinal plane, the separation

streamline between the fluid which flows around the obstacle and that which moves over it, occurs about 0.85 from the surface.

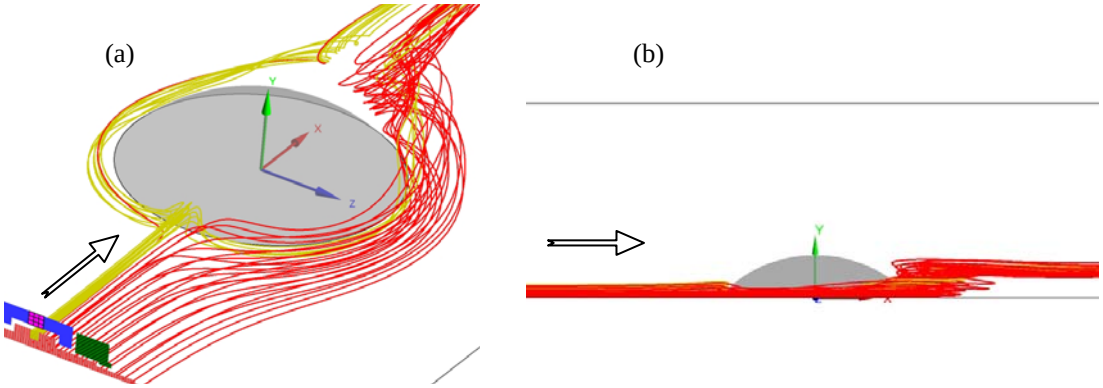


Figure 8. Flow passing through regions “a” (dark yellow stream) and “b” (red stream) around and downstream of protrusion. (a) 3-D view, (b) Elevation.

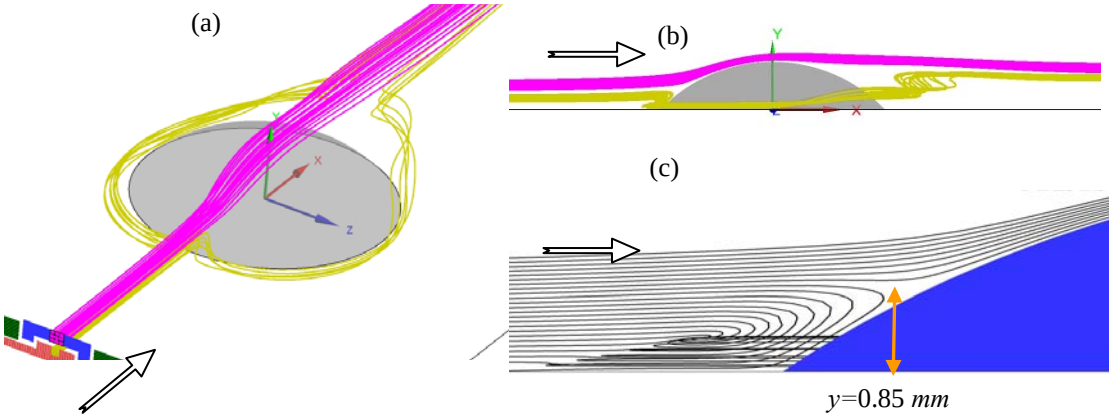


Figure 9. Flow passing through regions “a” (dark yellow stream) and “c” (pink stream) around and downstream of protrusion. (a) 3-D view, (b) Side view (c) Flow separation upstream of protrusion.

As mentioned above, and shown in Figure 8(b), the fluid crossing both regions “a” and “b” (Figure 5), exits the separation region downstream of the protrusion at a height of 1.5 , which is higher than their vertical position upstream of the protrusion. Interestingly, as shown in Figure 10, a portion of the fluid which initially passed through region “d”, coloured blue in Figure 5 and located above regions “a” and “b”, “fills the gap” left by the fluid which passed through “a” and “b” downstream of the obstruction. The fluid which passed through region “d” flows around the protrusion between the fluid streams from regions “b” and “c”, as shown in Figure 10(c). Downstream of the protrusion it flows along the separated region behind the protrusion, and as may be seen in Figures 10(a) and 10(b), wraps itself below the lifted flow from regions “a” and “b” thereby filling the region just above the lower wall. As shown in Figure 11(a), the fluid which passes through, region “f”, the thin area extending from 1 on either sides of the centre longitudinal plane up to the end of region “b” and located above region ‘b’ but below regions ‘d’ and ‘e’, fills the small gap between the lower wall and the stream which originated from region “d”. Further, as presented in Figure 11(b), the fluid which originally flowed through region “f”, wraps itself around the sides of the protrusion and the protrusion wake and then forms a thin vertical streams in the centre longitudinal region, at about 12.5 from the origin, keeping the fluid which passes at low level upstream of the protrusion close to the surface downstream of the protrusion.

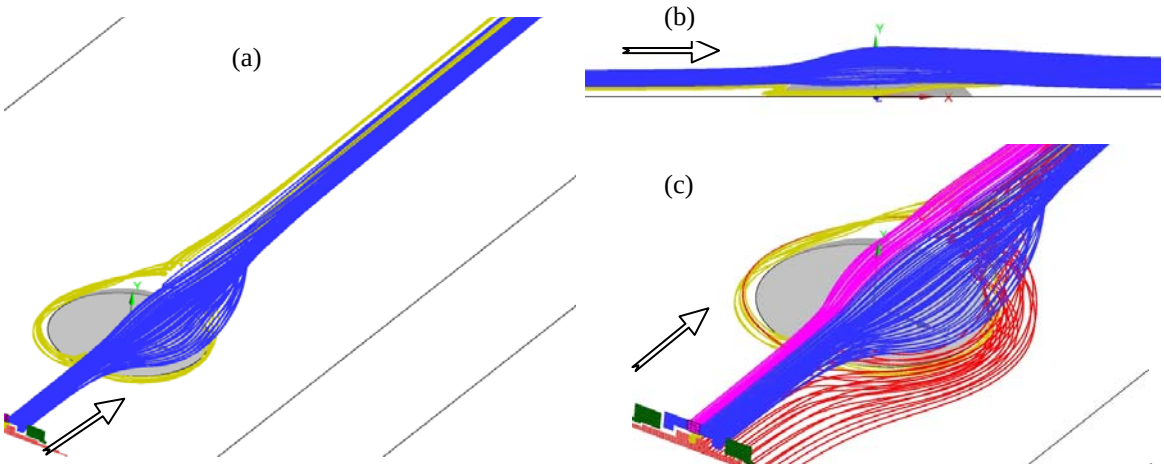


Figure 10. Flow passing through regions “a” (dark yellow stream) and “d” (blue stream) around and downstream of protrusion. (a) 3D view, (b) elevation. (c) 3D view.

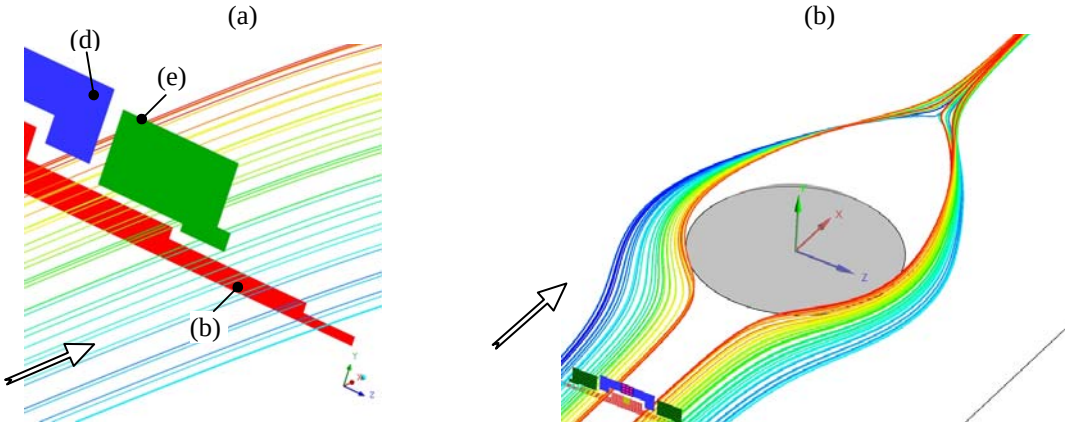


Figure 11. Flow passing through region “f” (each streamline indicated by different color) and passing between regions “d”, “e” and “b” (a) 3-D view around the regions, (b) 3-D view showing protrusion.

Finally, the flow which passes through region “e” (Figure 5), wraps itself outside of the fluid stream which passes through region “d”, around the protrusion sides and the separation region downstream of the protrusion. Downstream of the separation region this fluid stream spreads along the bottom wall, as may be seen in Figure 12.

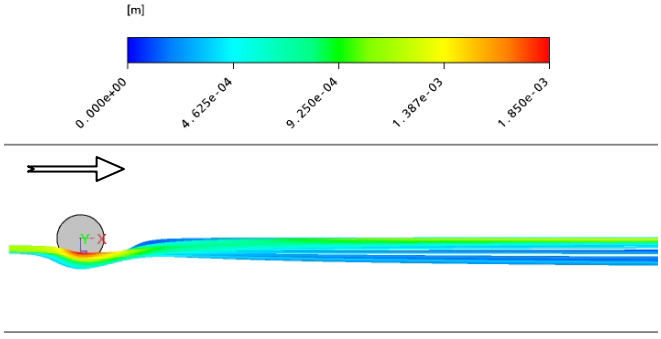


Figure 12. Side view of flow passing through region “e” (colored by vertical distance from bottom wall).

Now that the flow field has been has been described in some detail it is possible to discuss the concomitant temperature and heat transfer distributions.

**Heat Transfer** Four regions of high heat transfer rate generated from a protrusion in a channel can be seen in Figure 13. The highest rate of heat transfer is the region on the front surface in which of the protrusion where cold fluid from regions “a”, “b”, “c” and “d”, not yet heated by the hot bottom wall, approaches the heated surface of the protrusion. This accelerating fluid reduces the boundary layer thickness, thereby increasing the local temperature gradient with a consequent augmentation in the local heat flux, as may be seen in more detail in Figure 14.

Another region of increased heat transfer rate shown in Figure 13, is located near the upstream intersection between the protrusion and the lower channel wall. As mentioned above, the fluid which passes through region “a” is forced to change its direction and moves toward the bottom surface. The movement of cold fluid toward the bottom surface disturbs the thermal boundary layer and, as can be seen in Figures 15 and 16, increases the heat transfer rate on the channel lower wall immediately upstream of the protrusion.

Since the flow separation occurs, the rear of the protrusion is perforce located in the separated flow region. It might be therefore expected that there would not be any regions of high heat transfer on the rear of the protrusion. However, as can be seen in Figure 13 and in greater detail in Figure 17(a), there is a small area of high heat transfer on the back of the protuberance and at the centre of the lower channel surface close to and downstream of the protrusion.

This can be explained from the fact that cold fluid, which had passed through region “b” in Figure 5, enters, as is presented in Figure 17(b), the region of separated flow close to the bottom wall and a little downstream from the protrusion. It is then drawn towards the centre plane of the channel and as a consequence of the very low pressure behind the obstacle (Figure 7) the axial velocity is reversed so that fluid now approaches the protrusion from the downstream direction. Streamlines representing a portion of the flow through to region “b”, coloured with vertical distance from the bottom wall, are shown in Figure 17(b). Although the fluid moving towards the reer side of the protrusion enters the zone of separated fluid from a region close to the bottom surface of the channel, its velocity is sufficiently large and its temperature sufficiently low to slightly increase the heat flux on the lower surface of the channel. After this jet of fluid impacts into the rear of the obstacle, it is forced to flow upwards along its surface. The resultant increase in velocity, in what would otherwise have been an essentially stagnant region, leads to a significant enhancement of the local heat flux.

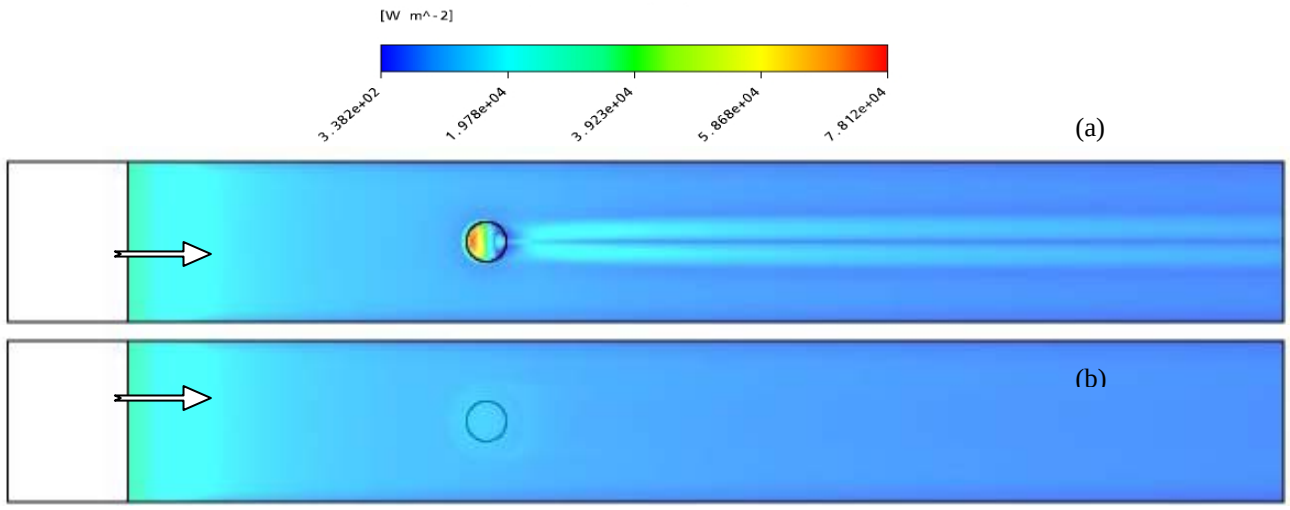


Figure 13. Heat flux distribution along the (a) protruded surface and (b) top wall.

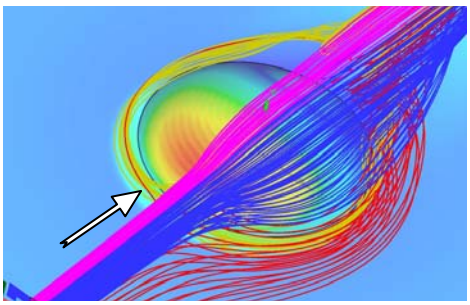

Figure 14. The protruded surface colored by heat flux and flow passing through regions “a”, “b”, “c” and “d”.

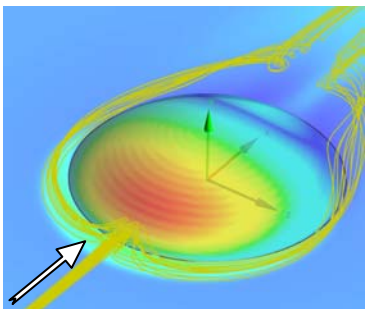

Figure 15. The protruded surface colored by heat flux and flow passing through region “a”.

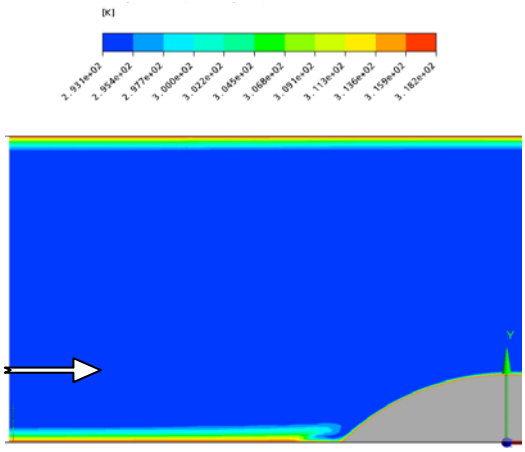

Figure 16. Temperature distribution at centre longitudinal plane upstream of protrusion.

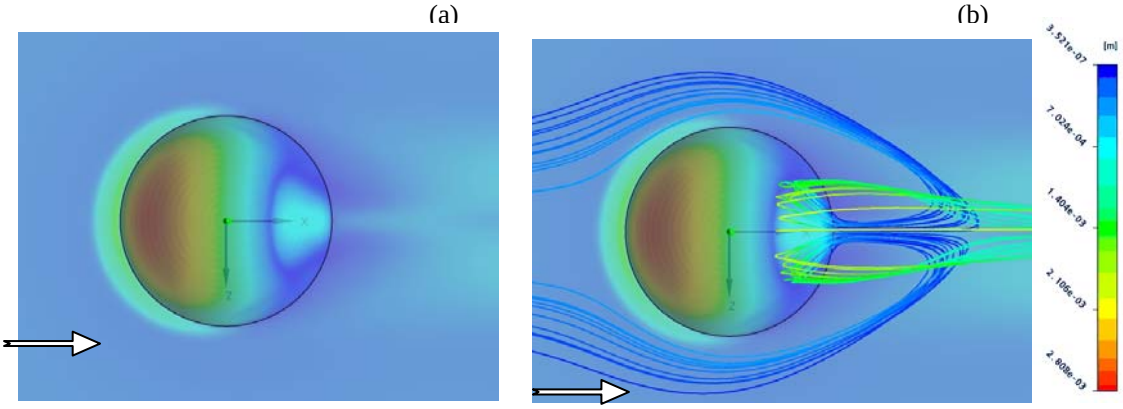


Figure 17. Heat flux distribution (a) protruded surface (b) streamlines, colored by vertical distance from bottom wall of the channel, of the fluid which initially passed through region “b”.

As shown in Figure 13(a), the fourth region of heat flux is located downstream of the separated flow region and consists of two strips on the lower surface of the channel. It can be related to two cool ribbons of fluid which, as discussed above, are formed by the fluid that had originally passed

through region “e”. Because the flow is laminar, there is no mixing unless there is significant vortical action

From the velocity and temperature distributions shown in Figure 18 it can be seen that the disturbance generated by the small protrusion only slightly disturbs the flow and temperature fields downstream of it. In fact, as is revealed in Figures 18(a) and (b), in the region immediately downstream of the obstruction there is very little cross flow so that no mixing of the hot and cold steams occurs. As the flow in the wake is accelerated by viscous action of the faster moving fluid around it, some material is necessarily transported towards the axis of the channel. Since the flow is laminar, diffusion of the velocity is rather slow, so that the resultant very low transverse velocities lead to the formation of similarly weak vortical structures which can be observed in Figures 18(c) and (d). It follows that there is hardly any mixing so that the two ribbons of fluid (see figure 10) which originally passed through region “d” and indicated by the white steaks on either side of the axial centreline of the lower surface of the channel in Figure 13(a), persists until the exit from the calculation domain. A low heat transfer region, designated in Figure 13(a) by the dark blue area around the longitudinal axis of the bottom wall of the conduit, results from the hot fluid which had originally gone through region “f”, being forced adjacent to the lower boundary of the channel (see Figure 10) .

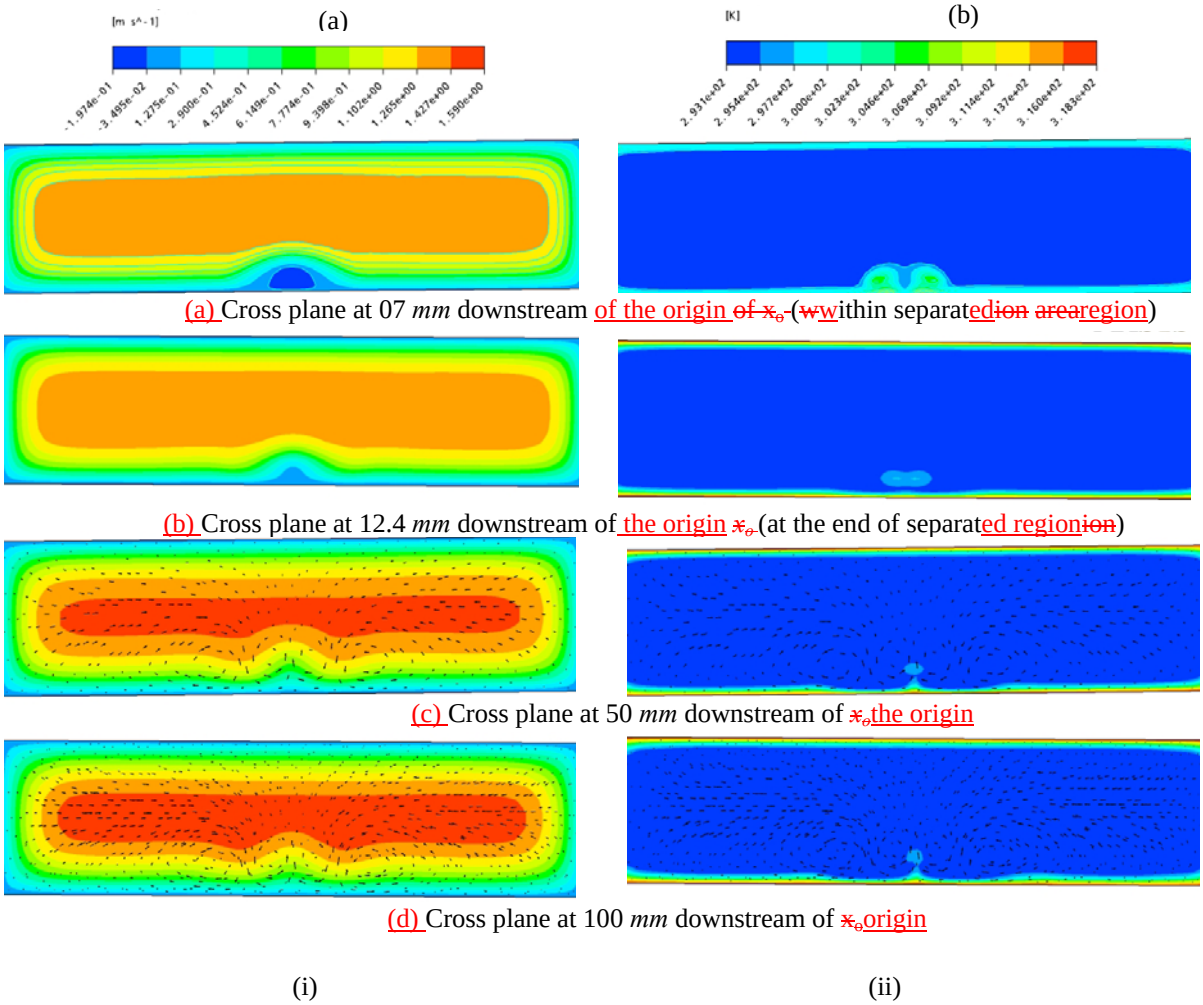


Figure 18. Contours of (i) axial velocity and (ii) temperature distributions at different cross planes. Also shown are cross-flow velocity vectors.

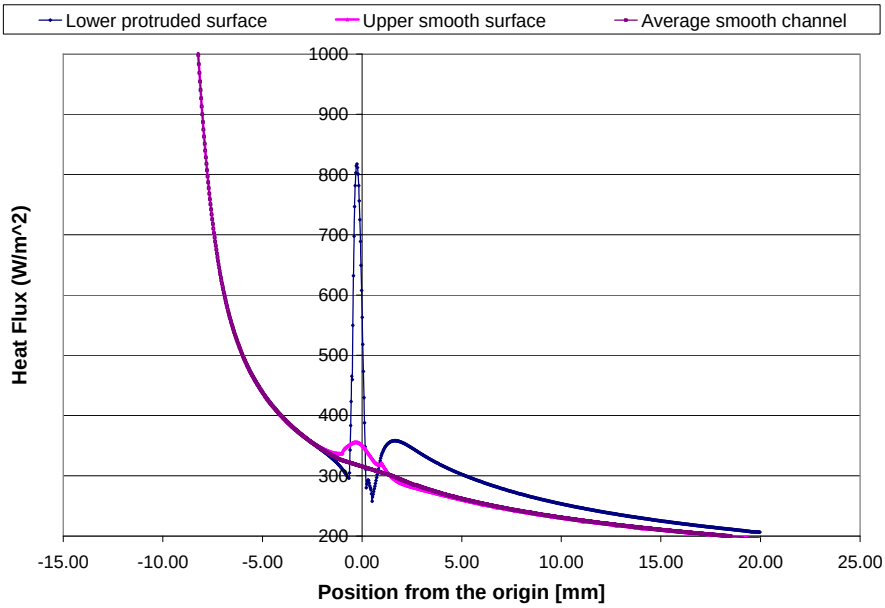


Figure 19. Heat flux as function of position on both upper and lower surfaces of the protruded channel, and the average for both upper and lower surfaces of the smooth channel.

The fact that there is very little mixing downstream of the small protrusion is clearly shown in Figure 19 since the heat flux about five diameters downstream of the protrusion on the lower face of the channel, corresponding to the cross-sectional flow shown in Figure 18(c), is only marginally greater that the heat flux which is obtained in a plane channel. The fact that the heat transfer on the top channel surface is barely affected by the presence of the obstacle, shown in Figures 13(b) and 19, also illustrates the lack of general mixing generated by the obstruction.

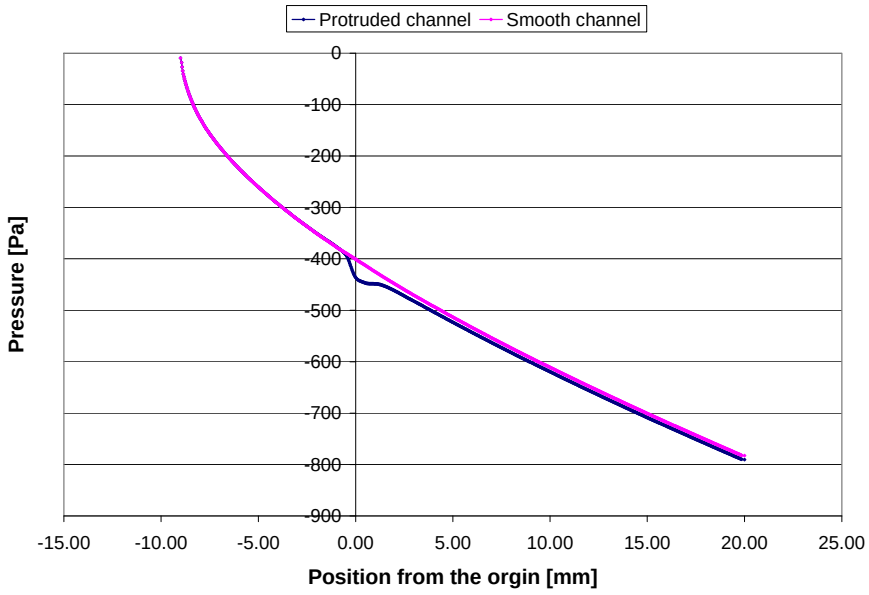


Figure 20 Pressure distribution in channel with and without protrusion.

The presence of the protrusion thus results in a small enhancement of 7% in the heat transfer rate in the whole channel. A measure that indicates, albeit imperfectly, the overall improvement in performance of a heat transfer device, is the performance index, $f'$, defined as

$$f = (q' / \Delta p) / (q_0' / \Delta p_0) \ , \qquad (4)$$

in which $q'$ and $\Delta p$ are the total heat transfer and pressure loss, respectively, and the subscript $o$ indicates the plane channel. Surprisingly, as may be seen in Figure 20, since the pressure drop increases by only 1%, $f$ increases by 6%. This marginal improvement in the performance index indicates that this small obstacle is not an effective means of enhancing heat transfer in heat exchanger channels.

## CONCLUSION

The flow around a heated protrusion on the hot wall of a channel is described in detail. The complex flow fields are used to explain the heat flux distribution on the protrusion and the channel walls. It is shown that the protrusion gives an enhancement in the heat transfer rate, which, because of the even smaller increase in the pressure drop leads to a 6% increase in the performance index.


### Acknowledgments

The authors would like to acknowledge with thanks the financial support of the Australian Research Council, grant DP0558903.


## REFERENCES


Alshroof, O., Reizes, J., Timchenko, V. and Leonardi, E., [2007], Numerical Evaluation of Heat Transfer from a Spherical Dimple in a Flat Plate: Development of Appropriate Boundary Conditions, *ASME International Mechanical Engineering Congress and Exposition, 11-15 Desember 2007 Seattle*, Washington, USA.

Belen'kiy, M., Gotovskiy M., [1991], Experimental Investigation of Heat and Hydraulic Characteristics of Heat Transfer Surfaces Formed by Simi-Spherical Cavities, *High Temperature*, Vol. 29, No. 6, pp 1142-1147.

Ekkad S. V., Nasir H., 2003, Dimple Enhanced Heat Transfer in High Aspect Ratio Channels, *Journal of Enhanced Heat Transfer,* Vol. 10, No. 4, pp 395-406.

Hwang, SD. and Cho, HH. [2007], Heat transfer enhancement of internal passage using dimple/protrusion, *13th International Heat Transfer Conference, HTE-24, **13**-14 July 2007 Sydney*, Australia.

Isaev S., Leontiev, A., Usachev A. and Frolov D., [1997], Numerical Simulation of Laminar Incompressible Three – Dimensional Flow Around a Dimple (Vortex Dynamics and Heat Transfer), *Russian Ministry of Science and Technologies,* Institute for High Performance Computing and Data Bases, Vol. 97. No. 6, pp 1-21.

Isaev, S., Baranov, P. and Usachov, A., [2001], Numerical Analysis of the Effect of Viscosity on the Vortex Dynamics in Laminar separated Flow Past a Dimple on a plate with Allowance for its Asymmetry, *Journal of Engineering Physics and Thermophysics*, Vol 74, No. 2, pp 339-346.

Khalatov, A., Byerley, A., Ochoa, D., Min, S-K. and Vinsent, R., [2004], Application of advanced Techniques to Study Fluid Flow and Heat Transfer Within and Downstream of a Single Dimple, *Proceedings of V Minsk International Heat & Mass Transfer Forum, 24-28 May 2004,* **Minsk.**

Leontiev, A., Gortyshov, Yu., Popov, I. and Olimpiev, V., [2006], Hydrodynamics And Heat Transfer in Heat Exchanger Channels With Spherical Holes, *ASME International Mechanical Engineering Congress & Exposition.. Nov 05-10, 2006, Chicago,* Illinois, USA.

Ligrani, P., Mahmood, G., Harrison, J., Clayton, C. and Nelson, D., [2001], Flow Structure and Local Nusselt Number Variations in a Channel with Dimples and Protrusions on Opposite Walls, *International Journal of Heat and Mass Transfer,* Vol. **44** , No. 23, pp 4413–4425.

Mahmood, G. I., Hill, M. L., Nelson D. L, Ligrani P. M., Moon, H.-K. and Glezer B., 2001, Local Heat Transfer and Flow Structure on and above a Dimpled Surface in a Channel, *Trans. ASME, J. Turbomachinery*, Vol. **123** No. 1, pp 115–123.

Mahmood, G. I. Sabbagh, M. Z. and Ligrani, P. M., [2001], Heat Transfer in a Channel with Dimples and Protrusion on Opposite Walls*, Journal of technology and heat transfer,* Vol. 15, No. 3, pp 275–283.

Mahmood, G. I. and Ligrani, P. M., [2002], Heat Transfer in a Dimpled Channel: Combined Influences of Aspect Ratio, Temperature Ratio, Reynolds Number, and Flow Structure, *Int. J. Heat Mass Transfer*, Vol. **45** No. 10, pp 2011–2020.

Terekhov, V. I., Kalinina S. V. and Mshvidobadze, Y. M., [1997], Heat Transfer Coefficient and Aerodynamic Resistance on a Surface with a Single Dimple, *Enhanced Heat Transfer*, Vol. 4, pp 131–145.

Wang, Z., Yeo, K. and Khoo, B., [2003], Numerical Simulation of Laminar Channel Flow Over Dimpled Surface, *23-26 June 2003 AIAA, Orlando*, Florida.